Strong climate coupling of terrestrial and marine environments in the Miocene of northwest Europe

T.H. Donders [a,c,*], J.W.H. Weijers [b,1], D.K. Munsterman [c], M.L. Kloosterboer-van Hoeve [a,e], L.K. Buckles [d], R.D. Pancost [d], S. Schouten [b], J.S. Sinninghe Damsté [b], H. Brinkhuis [a]

[a] *Palaeoecology, Laboratory of Palaeobotany and Palynology, Utrecht University, Budapestlaan 4, 3584 CD Utrecht, The Netherlands*
[b] *Department of Marine Organic Biogeochemistry, NIOZ Royal Netherlands Institute for Sea Research, PO Box 59, 1790 AB Den Burg — Texel, The Netherlands*
[c] *TNO B&O, Geological Survey of The Netherlands, P.O. Box 80015, 3508 TA Utrecht, The Netherlands*
[d] *Organic Geochemistry Unit, Bristol Biogeochemistry Research Centre, School of Chemistry, Cantock's Close, Bristol University, Bristol BS8 1TS, UK*
[e] *Goois Lyceum, Vossiuslaan 2a, 1401 RT Bussum, The Netherlands*

ABSTRACT

A palynological and organic geochemical record from a shallow marine paleoenvironmental setting in SE Netherlands documents the coupled marine and terrestrial climate evolution from the late Burdigalian (~17 Ma) through the early Zanclean (~4.5 Ma). Proxy climate records show several coeval variations in both relative sea surface (deduced from percent cool dinocysts) and terrestrial (subtropical vs. cool temperate pollen) temperature indices. The terrestrial climatic trend is confirmed by a quantitative reconstruction of annual mean air temperature based on the distribution of fossil branched glycerol dialkyl glycerol tetraethers, showing a cooling from ~27 °C to ~14 °C between 17 and 5 Ma punctuated by short-term variations. Decreases in sea surface temperature broadly correlate to inferred third-order sea level variations and correspond to isotope glacial events Mi-3 through Mi-7. An additional strong SST decrease occurs around ~8.4 Ma, coincident with a strong reduction and regional disappearance of subtropical pollen types. This cooling phase seems associated with lowered sea levels, but it has not yet been described from the deep sea δ^{18}O record.

© 2009 Elsevier B.V. All rights reserved.

1. Introduction

1.1. Miocene climate evolution

The Cenozoic climate evolution based on marine deep sea records is relatively well known since continuous well-dated records are available (e.g. Flower and Kennett, 1994; Zachos et al., 2001; Holbourn et al., 2005; Zachos et al., 2008). For the Miocene, the most characteristic features are the mid-Miocene climate optimum between 17 and 15 Ma, followed by gradual cooling and a series of distinct glacial stages (Miller et al., 1991, 1996). In contrast, the Cenozoic evolution of terrestrial climate is still poorly known, especially concerning the amplitude and timing of changes relative to the marine climate record. The most comprehensive long-term continental palaeoclimate reconstruction available covers mean annual and seasonal temperature and precipitation for the last 45 million years (Ma) and was established by comparing plant macrofossil assemblages to present distributions of extant species in Europe (Mosbrugger et al., 2005). The authors tentatively correlated their reconstructed continental climatic trend with a global compilation of oxygen stable-isotope ratios in benthic foraminifera by Zachos et al. (2001). Although general trends are well reflected in both records, Mosbrugger et al. (2005) observe that their regional continental record lags the rapid cooling between 15 and 13 Ma as recorded in the global deep-sea temperature record of Zachos et al. (2001). A significant winter terrestrial temperature decrease in the Mosbrugger et al. (2005) record occurs only between 12 and 10 Ma, suggesting a decoupling between European continental and global marine climates.

To assess the precise temporal relationship between land and sea-based climate records, a higher temporal resolution than the Mosbrugger et al. (2005) record (>1 Ma sample^{-1}) is needed, particularly for the relatively short-term (<~0.5 Ma) glacial phases that have been recognized in the Neogene (see Miller et al., 1991). Thus, additional approaches should be explored to estimate pre-Pleistocene terrestrial environmental conditions and investigate the potential coupling between terrestrial and marine climatic changes in greater detail.

1.2. Proxy approach

Our approach is to integrate palaeoclimatic signals from middle Miocene to early Pliocene terrestrial and marine environments through quantitative palynological and organic geochemical analyses

---

* Corresponding author. TNO B&O, Geological Survey of The Netherlands, P.O. Box 80015, 3508 TA Utrecht, The Netherlands. Tel.: +31 30 2564566.
E-mail address: timme.donders@tno.nl (T.H. Donders).
[1] Currently at: Department of Geosciences, Utrecht University, The Netherlands.

Table 1
Dinocyst taxa grouping.

Restricted and coastal dinocysts	Cold water Arctic dinocysts
Acanthaulax miocenicum	Bitectatodinium tepikiense
Achomosphaera andalousiensis	Filisphaera filifera
Apteodinium australiense	Habibacysta tectata
A. conjuctum	'Headinium miocenicum' (**)
A. emslandia	
A. granulatum	
A. spiridoides	
A.tectatum	
A. tectum	
Areoligera semicirculata	
Chiropteridium galea	
C. lobospinosum	
Cordosphaeridium cantharellus	
C. gracile	
C. minimum	
Cyclopsiella granulose	
Dapsilidinium spp.	
Glaphyrocysta exuberans	
Gramocysta verricula	
Heteraulacacysta campanula	
Homotryblium floripes	
H. oceanicum	
H. plectilum	
H. tenuispinosum	
H. vallum	
Mendicodinium robustum	
Operculodinium israelianum	
Paralecaniella spp.(*)	
Polysphaeridium congregatum	
P. zoharyi	
Spiniferites cruciformis	
Systematophora placacantha	
Thalassiphora pelagica	
Toenisbergia spp.	
Tuberculodinium vancampoe	

(*) The marine acritarch *Paralecaniella* sp. is typical of restricted marine conditions (Brinkhuis and Schiøler, 1996).
(**) Manuscript name, Zevenboom (1995).

of a set of near-continuous marginal marine sedimentary archives from the North Sea Basin. Coupled analysis of pollen as well as organic-walled dinoflagellate cyst (dinocyst) assemblages are combined with analyses of fossil glycerol dialkyl glycerol tetraether (GDGT) core membrane lipids derived from marine Crenarchaeota and soil bacteria. This multi-proxy approach yields a relatively detailed continental and marine palaeoenvironmental record for the NW European Miocene, and provides detailed insight into the degree of land-sea coupling during the build up of continental ice sheets (see e.g. Miller et al., 1991; Flower and Kennett, 1994; Zachos et al., 2001, 2008).

Pollen and spores provide a reliable source of terrestrial paleoenvironmental and -climatic information (Birks and Birks, 1980). Despite their sensitivity to climate changes, terrestrial (pollen) records are often associated with chronostratigraphical problems, high spatial variability, and discontinuous accumulation (Pross and Klotz, 2002; Kemna and Westerhoff, 2007; Donders et al., 2007). Shallow marine sedimentary archives can resolve the problems associated with continental-based records, although differential transport by wind or water can bias the pollen assemblages. Assemblages with a relatively high number of taxa, including typical insect-pollinated forms, are indicative of substantial pollen input through water transport (Whitehead, 1983), in contrast to typical low-diversity wind-transported pollen (Hooghiemstra, 1988). For locations proximal to a river delta the majority of the pollen is likely water-transported. Once in the water column, lumping of dust particles (including pollen) into fecal pellets near the sea surface causes accelerated sinking and prevents marked lateral transport by ocean currents (Hooghiemstra, 1988).

The preference of dinoflagellates for neritic conditions enables a synchronous reconstruction of marine and terrestrial palaeo-environments. Species–environment relations can be empirically deduced from comparisons with other fossil groups or physical and chemical evidence, as well as by comparing distributions of extinct taxa with species for which the ecology is better known (Versteegh and Zonneveld, 1994; Sluijs et al., 2005). Sea surface temperatures (SSTs) and different inshore to offshore water mass conditions (e.g. Brinkhuis, 1994; Versteegh and Zonneveld, 1994) can thus be deduced from pre-Quaternary dinocyst assemblages (e.g. see Sluijs et al., 2005; Pross and Brinkhuis, 2005) (see Table 1). Water mass conditions, in turn, depend on sea-level variations, which can thus be detected using relative changes in the dinocyst assemblages.

Branched GDGT membrane lipids are presumably derived from anaerobic soil bacteria (Weijers et al., 2006a,b) and isoprenoid GDGTs are mainly derived from marine pelagic Crenarchaeota in marine sediments (e.g. Schouten et al., 2000). The Branched and Isoprenoid Tetraether (BIT) index is a measure for the relative fluvial input of soil organic matter in marine sediments (Hopmans et al., 2004; Weijers et al., 2006b). Further, the relative distribution of branched GDGT membrane lipids in soils, expressed in the Methylation index of Branched Tetraethers (MBT) and the Cyclisation ratio of Branched Tetraethers (CBT), is a function of annual mean air temperature (MAT) and soil pH (Weijers et al., 2007b).

2. Geological setting

A complex Cenozoic rift system of approximately 1100 km extends from the west coast of The Netherlands through western Germany and southeastern France towards the western Mediterranean. The rift formed to accommodate stress from the Alpine orogeny, and (in NW Europe) during the Neogene consists of the Roer Valley Graben, Lower Rhine Embayment and Leine Grabens (Fig. 1a) (Ziegler, 1994; Geluk et al., 1994). The Roer Valley Graben (RVG) rift system is the main structural–physiographic unit of the Lower Rhine Embayment and is differentiated into several tectonic units (Van den Berg, 1994). Significant differential subsidence started in the late Oligocene across the re-activated Peel Boundary Fault (Geluk et al., 1994). During the Miocene, the northeastern Venlo Block (VB) of the RVG was a shallow marine environment in the proximity of terrestrial environments (Fig. 1b) (Ziegler, 1994), receiving an influx of both marine and terrestrial organic microfossils. Relatively slow and stable subsidence, combined with a warm and humid climate led to widespread peat accumulation from the Burdigalian to Serravallian or lower Tortonian in parts of the RVG (Lücke et al., 1999; Utescher et al., 2000). The thick peat deposits formed about 100 m of lignite, while minor coal seams formed during the Tortonian–Messinian (Zagwijn and Hager, 1987; Lücke et al., 1999). These swamp ecosystems are the main source of terrestrial organic material such as pollen and spores in the southern North Sea sedimentary record. The Massif Central–Rheinish Massif uplift, separating the northern and southern Rhine Grabens, started during the early Miocene and continued into the Plio-/Pleistocene (Ziegler, 1994). Hence, any sites on the VB accumulate material from the relatively restricted Northern Rhine Graben catchment throughout the Miocene.

3. Materials and methods

3.1. Site description and sampling

Two airlift cores from the RVG in the SE Netherlands (Fig. 1), the Groote Heide (GH) and Heumensoord (HEU) boreholes, span the upper part of the Miocene Breda Formation that consists of glauconitic sands, sandy clays and clays (Doppert et al., 1975). The GH core also covers the lower part of the overlying fluviatile, mostly Pliocene, Kieseloöliet formation (Zagwijn and Hager, 1987), and was here studied for dinocysts,
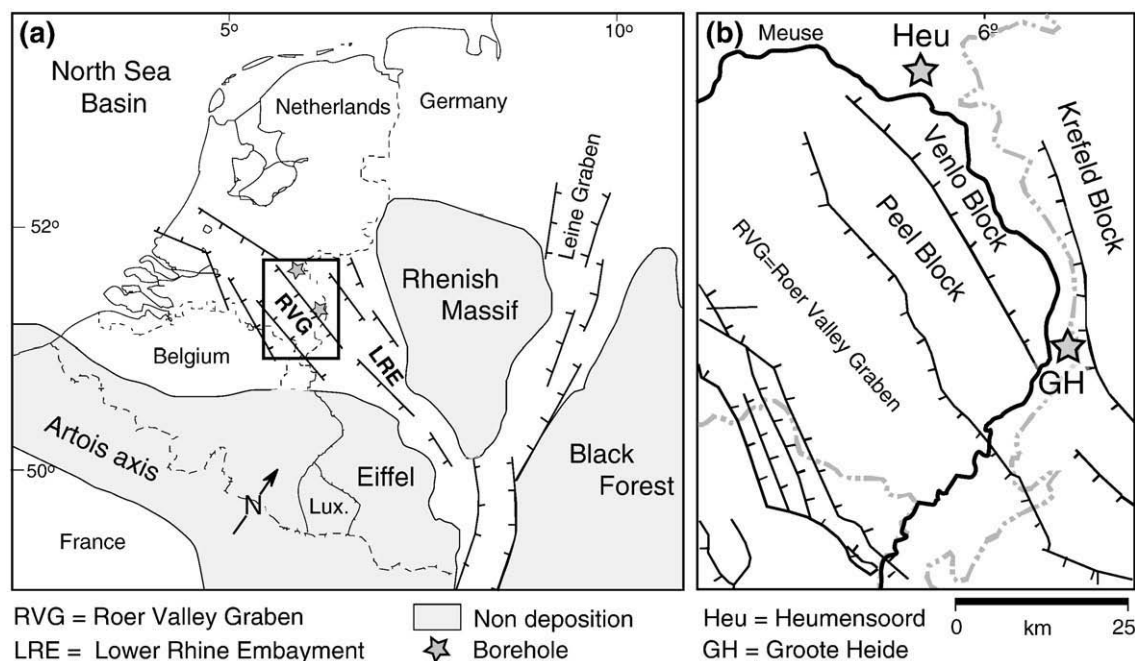
Fig. 1. (a) Overview of NW Europe with Miocene palaeogeography (after Ziegler, 1994) (b) Structural framework of the Roer Valley Graben and the GH and HEU site locations (after Geluk et al., 1994).

pollen and spores, GDGT lipids, and physical properties. Due to the more distal position, the HEU borehole (Fig. 1b) is less likely to contain hiatuses related to sea level lowstands. The HEU site provides a more complete sedimentary record and is best suited for past SST reconstructions. This borehole was studied for dinocysts and physical properties. The airlift coring method provides mixed samples from 1–2 m intervals. Therefore, reconstructed sea-level and climatic variations represent smoothed trends within a relatively expanded sedimentary record.

3.2. Palynological methods

Palynological processing of 54 samples was done according to standard methods (e.g. Wood et al., 1996) involving HCl–HF–HCl digestion, and sieving over 18 μm and 10 μm mesh for dinocysts and pollen samples respectively. For the dinocyst analyses, heavy minerals were removed by flotation over zinc chloride ($ZnCl_2$, specific gravity: 2.1 g/cm^3). Dinocysts and pollen/spores were examined independently by light microscopy and counted up to ~150 identified cysts (an additional slide was scanned for rare taxa), and ~300 pollen/spores. Dinocyst taxonomy follows that cited in Fensome and Williams (2004), and pollen and spore taxonomy is based on Menke (1976), Mohr (1986), and Stuchlik (2002).

As the GH and HEU borehole locations are proximal to the palaeo-Rhine delta the majority of the pollen is likely to be water-transported. To preclude large shifts in the pollen assemblages due to changes in proximity to the coast, predominantly wind-transported bisaccate pollen, mostly *Pinus*, were excluded from the pollen percentage sum. In this way, *Pinus* abundances are expressed relative to the total of all other pollen and spores (i.e. the pollen sum) but do not influence relative abundances of taxa within the pollen sum.

We used Gonyaulacoid dinocysts as the principal marine paleoenvironmental proxy because their distribution is highly sensitive to changes in e.g. sea-surface temperature (SST), salinity (SSS), water mass and productivity (e.g. Dale, 1996; Pross and Brinkhuis, 2005; Sluijs et al., 2005). Following approaches of e.g. Brinkhuis (1994) and Dybkjær (2004), we compared several relative indices based on palynomorph abundances to detect third-order sea-level maxima. A highly sensitive indicator for sea level changes is the abundance of restricted and coastal marine dwellers (see Table 1) relative to the total amount of

Gonyaulacoid dinocysts (see e.g. Brinkhuis, 1994; Stover et al., 1996; Dybkjær, 2004; Pross and Brinkhuis, 2005; Sluijs et al., 2005). In addition, the amount of pollen relative to dinocysts indicates the relative distance to the coast, since pollen represents input of terrestrial material. Since bisaccate pollen, relative to other pollen, are dispersed along large distances due to good floating and wind-dispersal capability they are excluded from the index (Traverse, 1988; Hooghiemstra, 1988). Dinocysts indicative of cool conditions can also point to sea level variations since glacio-eustatic cycles correlate with temperature. Sea-level lowstands are most marked by (short) unconformities in the shelf sediments. Relative to GH, HEU is the more offshore and expanded record, and likely contains a more complete record of SST and associated sea level variations.

3.3. GDGT membrane lipids

For analysis of GDGT lipids in selected samples, about 10–20 g of freeze dried sediment was ground and ultrasonically extracted using successively less polar solvents (methanol, methanol:dichloromethane (DCM) 1:1 (v/v), and DCM), 3 times for 5 min each. The combined extracts were separated over an activated Al_2O_3 column into an apolar and polar fraction, using *n*-hexane:DCM 1:1 (v/v) and DCM:methanol 1:1 (v/v), respectively. The latter fraction, containing the GDGTs, was ultrasonically dissolved in *n*-hexane:propanol (99/1, v/v) and filtered over a 0.45 μm mesh PTFE filter (ø 4 mm) prior to analysis. GDGTs were analyzed using high performance liquid chromatography/atmospheric pressure chemical ionization–mass spectrometry (HPLC/APCI-MS) with an Agilent 1100 series/Hewlett-Packard 1100 MSD SL series instrument following methods of Hopmans et al. (2000, 2004). Injection volume of the samples was 10 μl. To increase sensitivity, selective ion monitoring (SIM) of the protonated molecular ions of the GDGTs was used (cf. Schouten et al., 2007). Relative quantification of the compounds was achieved by integrating the $[M+H]^+$ (protonated molecular ion) peaks in the mass chromatograms.

The BIT index for the relative fluvial input of soil organic matter in marine sediments ranges from almost 0, indicating pure marine derived organic matter, to nearly 1, pointing to a predominant terrestrial source of the organic matter (Hopmans et al., 2004; Weijers et al., 2006b). The calibration equations of the MBT and CBT are taken from Weijers et al.

(2007b); CBT = 3.33−0.38×pH and MBT = 0.122 + 0.187×CBT + 0.020×MAT. At marine sites with high terrestrial organic matter input, i.e. close to river outflows, this distribution can be used to reconstruct terrestrial MATs integrated over the river catchment (e.g. Weijers et al., 2007a). Reproducibility of the results in this study, based on pooled standard deviations of duplicate (at 2 intervals) and triplicate (at 4 intervals) sample processing, is 0.01 for the BIT index, 0.02 for the soil pH estimate and 0.6 °C for the annual MAT estimate.

4. Biochronostratigraphy and depositional model

Recently, a marine palynological zonation for the southern North Sea Miocene Basin was proposed partly based on analyses of sediments of the GH and HEU boreholes (Munsterman and Brinkhuis, 2004). The zonation is consistent with a recent overview of the stratigraphic dinocyst distribution in Germany (Köthe and Piesker, 2007), and

followed the Berggren et al. (1995) timescale (Munsterman and Brinkhuis, 2004) (supplementary Fig. 1; Table 1). We updated the North Sea dinocyst zonation of Munsterman and Brinkhuis (2004) to the recent astronomically-tuned Neogene time scale (ATNTS) (Lourens et al., 2004) (supplementary Fig. 1; Table 1). Although the Mediterranean dinocyst record is largely representative for the North Sea Basin, it is evident that not all correlations are isochronous (see discussion in Munsterman and Brinkhuis, 2004). Instead of producing an independent age-depth model for each site, we used the continuous γ-ray measurements and core descriptions to achieve optimal correlation between both sediment cores. The depositional model shows shifts in the accumulation rate between both sites. In the lower section (correlation points 10–6, Fig. 2) the average accumulation rate is slightly higher in GH than in HEU, whereas this situation is reversed for the upper section, indicating a shift in the position of the depositional center. The GH depths were converted to the HEU depth scale
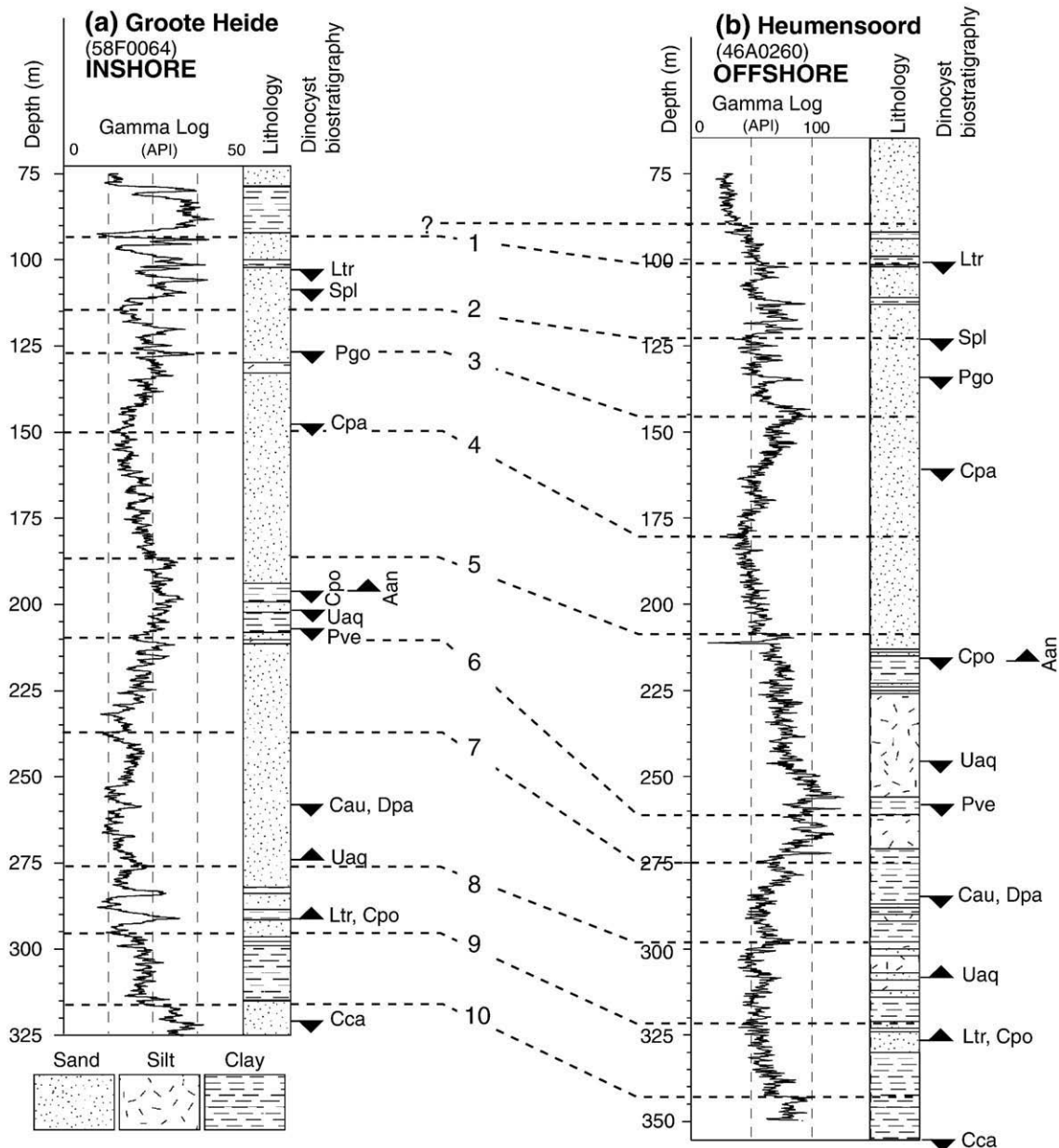

Fig. 2. Core descriptions, γ-ray logs and biostratigraphic dinocyst events sensu Munsterman and Brinkhuis (2004) of the GH and HEU boreholes. Dotted lines and numbers 1–10 refer to correlations of the γ-ray logs used for depth correlations between GH and HEU.
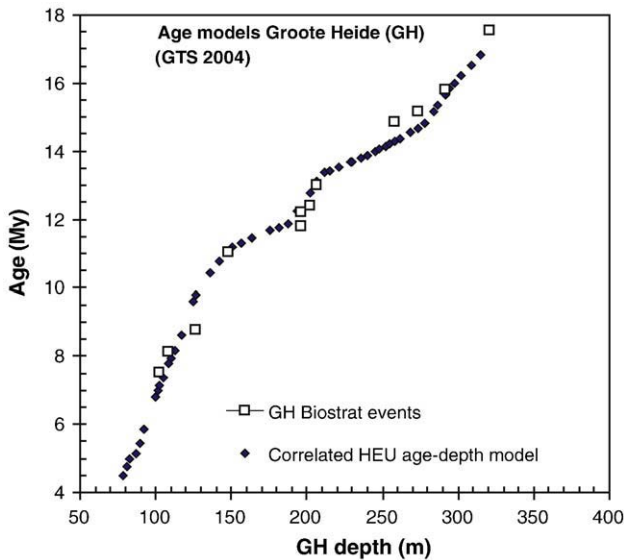
Fig. 3. Age depth models for GH. The independent model (large open squares) is based on GH biostratigraphic dinocyst events summarized in Table 2. The regional model (closed diamonds) is based on correlation to the HEU borehole (shown in supplementary Fig. 3) using the HEU biostratigraphic dinocyst events and polynomial age–depth interpolation.

(supplementary Fig. 2), whereby a regionally consistent single age–depth model for both sites could be defined (Fig. 3). The depositional model results in a mean sample interval of 0.2 Ma.

5. Proxy results

5.1. Terrestrial climate data

By relating fossil pollen taxa with their nearest living relative, following e.g. Suc and Zagwijn (1983), Huhn et al. (1997), and Fauquette et al. (1998), we interpreted the environment–taxa relations. A Principal Component Analysis (PCA) (Fig. 4) of the GH pollen assemblage data (see supplementary Fig. 3) revealed clear temperature and humidity-related gradients in the data. The first principal component (PC, Fig. 4) represents a gradient between subtropical (e.g. *Symplocos*, *Celtis*, *Engelhardtia*, *Tricolpites microhenrici*, *Tricolporites edmundi*, *T. megaexactus*) and temperate taxa (e.g. *Pinus*, *Betula*, *Fraxinus*, *Salix*, *Alnus*, Ericales). The second PC represents a gradient from relatively dry land plants (e.g. *Fagus*, *Carya*, *Ilex*, Ericales, Poaceae) to humid or swamp taxa (e.g. *Taxodium*, *Sequoia*, *Nyssa*, *Alnus*). The scores on the first and second PC of the samples are used as trends in relative terrestrial temperature (TT$_{pollen}$, Fig. 5d) and humidity (TH$_{pollen}$, Fig. 5e), respectively. The TT$_{pollen}$ shows three main cooling phases (I–III in Fig. 5) that are interrupted by periods of warming. However, the overall trend is toward cooler conditions.

BIT values for the Burdigalian and Langhian sediments vary between 0.57 and 0.83 and indicate a strong fluvial soil organic matter input to the sediments at GH (Hopmans et al., 2004) (Fig. 6). During the Serravallian and early Tortonian, BIT indices are clearly lower, varying between 0.33 and 0.64, but still indicative of considerable fluvial soil organic matter input. From the late Tortonian onwards, BIT values strongly increase to values around 0.90 in the Messinian and 0.99 into the Pliocene, with only relatively lower values (0.72–0.77) around the Tortonian/Messinian boundary. Reconstruction of absolute SSTs using the TEX$_{86}$ proxy, which is based on GDGTs derived from marine crenarchaeota (Schouten et al., 2002), is not possible as high amount of soil organic matter input at this location results in an input of GDGTs by soil crenarchaeota obscuring the aquatic TEX$_{86}$ signal (cf. Weijers et al., 2006b). The high amounts of branched GDGTs, however, do allow the use of the MBT/CBT proxy (TT$_{GDGT}$) to

infer annual MATs (Weijers et al., 2007b). The CBT component of this proxy, indicative of soil pH, shows relatively constant values throughout the record, i.e. ratios varying from 0.77 to 1.00. Using the transfer function derived from the global soil calibration set (Weijers et al., 2007b), this would correspond to average soil pH values for the drainage basin of the proto Rhine River ranging between 6.7 and 6.1, respectively, over this time interval. The MBT index, however, does show a considerable change, from values around 0.8 for the early Miocene down to values of 0.6 for the late Miocene and early Pliocene, and this clearly reveals a substantial cooling in the source region. Absolute temperatures over this Miocene interval were obtained with the CBT and MBT using the transfer function of Weijers et al. (2007b). From the Burdigalian to the middle Serravallian, the estimated annual MAT varies between 21 and 28 °C with a distinct peak in warmth just before the Langhian–Serravallian boundary. From the middle Serravallian onward, estimated MATs gradually decrease from ca. 23 °C down to ca. 14 °C in the Pliocene. Such absolute temperatures should be treated with caution, as several uncertainties regarding this new proxy remain, e.g., the source and ecology of the branched GDGT synthesizing organisms. It has also been shown that branched GDGT distributions for different locations might have a slightly different calibration towards soil pH and temperature (Sinninghe Damsté et al., 2008). Nevertheless, the overall cooling trend over the time interval investigated is clearly recorded by significant changes in the MBT/CBT proxy, corresponding to a shift of about 14 °C.

5.2. Marine climate and sea level data

The composition of the dinocyst assemblages suggests a strong Northern-Hemisphere temperate signal (e.g. Versteegh and Zonneveld, 1994; Dale, 1996; Head, 1998). Within this temperate assemblage, typical cold water Arctic taxa can be recognized (see Table 2) and these are grouped as indicator of cool SST in both GH (Fig. 5g) and HEU (Fig. 5h) (hereafter SST$_{dino}$). The SST$_{dino}$ records at both GH and HEU show a number of cool phases that increase in amplitude and duration. The first clear cool pulse around 13.8 Ma (IV in Fig. 5) is also present in the TT$_{GDGT}$ (see Section 5.1.) and TT$_{pollen}$, and is followed by a second
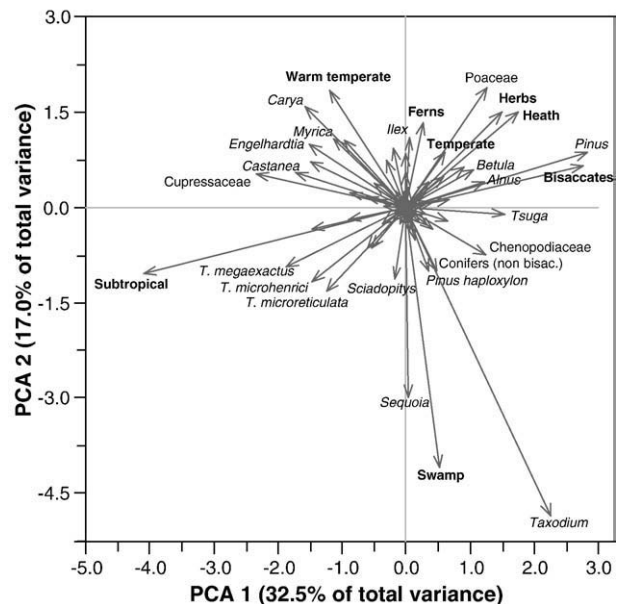

Fig. 4. Principal components analysis (PCA) biplot of the pollen percentage data of GH (Fig. 5). The plot shows a gradient from warm subtropical to cooler temperate species along axis 1, while axis 2 represents a wet (swamp) to dry (upland) vegetation gradient. T. = *Tricolporites*. Passive group scores are indicated with bold type and correspond to groups used in supplementary Fig. 2.
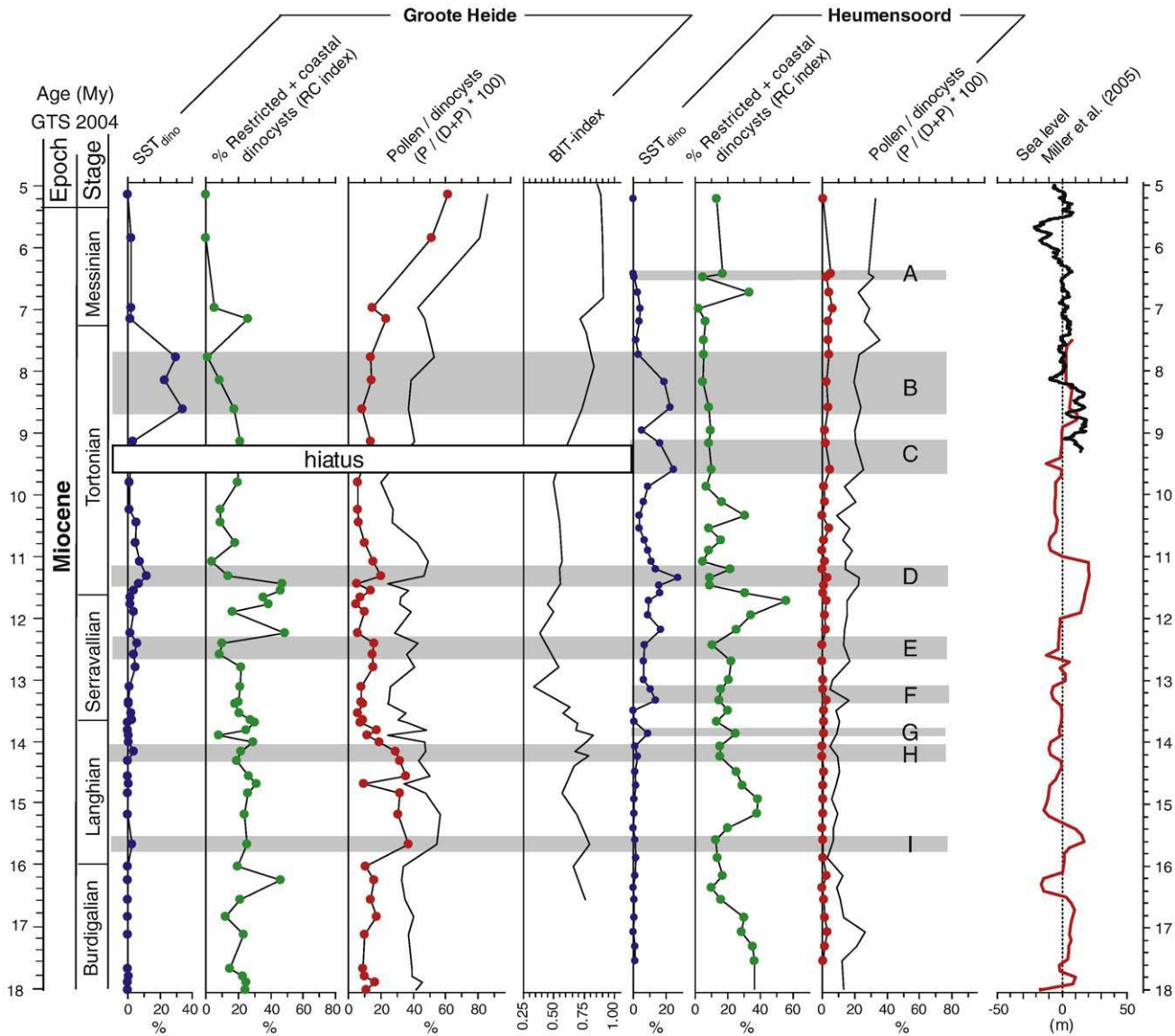
Fig. 5. (a, b) Terrestrial climate reconstruction by Mosbrugger et al. (2005), showing (a) cold month mean (CMM) and (b) mean annual precipitation (MAP) reconstructions based on macro-paleobotanical remains from the Lower Rhine and Lausitz/Weisselster Basins in, respectively, western and northern Germany. (c) MBT/CBT (TT$_{GDGT}$) proxy for terrestrial annual mean air temperature (MAT) on selected samples from GH. (d–h) Palynological proxies from the GH and HEU boreholes of terrestrial pollen-based temperatures (TT) and humidity (TH), relative amount of terrestrial palynomorphs ($P/(D+P)*100$), and dinocyst-based sea surface temperature changes (SST$_{dino}$) Shaded horizontal bars indicate cool phases in both the GH and HEU SST$_{dino}$ record. (i) Benthic $\delta^{18}O$ stages of Miller et al. (1991, 1996). The original age model for site 608 is here updated by correlating geomagnetic polarity reversals from site 608 (Miller et al., 1986) to the astronomically tuned Neogene timescale (Lourens et al., 2004). (j) Confirmed and orbitally tuned Miocene (Mi-) glacials. The Mi-glacials as identified by Miller et al. (1991, 1996) have been difficult to recognize and confirm in high-resolution benthic stable isotope records (Andersson and Jansen, 2003). However, several of these events have been identified in orbitally tuned records by Shackleton et al. (1999), Turco et al. (2001), Abels et al. (2005), and Westerhold et al. (2005). The orbitally tuned ages of Mi-3b at 13.82 Ma, Mi-5 at 11.4 Ma, and the Mi-6 at 10.4 (J) are coincident with ~1.2 Ma obliquity amplitude and eccentricity minima (Turco et al., 2001; Abels et al., 2004). However, the position of Mi-5 is disputed, and also two possible timings for Mi-7 have been proposed (J) (Westerhold et al., 2005).

Fig. 6. GH and HEU records of SST$_{dino}$ (blue circles), total pollen relative to dinocyst abundance (P/D index) without (red circles) and with (black line) bisaccate pollen, and abundance of restricted and coastal dinocysts relative to all gonyaulacoid dinocysts (RC index, green circles). For GH also the BIT index is shown with 0 indicating marine and 1 indicating terrestrial conditions (Hopmans et al., 2004). Letters A–I refer to inferred levels of low sea level based on the indices presented (see Section 6.2). A comparison with the global eustatic sea level reconstruction from Miller et al. (2005) is made, with the red curve showing back-stripped data and the thick black line representing a 20-point running mean of stable oxygen isotope measurements corrected for temperature.

cooling at 13.3 Ma. The other cool pulses broadly occur in two phases; the first between 13.5 and 11 Ma and the second between 9.5 and 7.5 Ma (marked V and VI in Fig. 5). These phases of enhanced cooling parallel the long-term cooling trends in the TT$_{pollen}$ (II and III in Fig. 5). A notable difference between the TT$_{pollen}$ and SST$_{dino}$ temperature trends is the marked ending of the main cool pulse in the SST$_{dino}$ record around 7.5 Ma, while the TT$_{pollen}$ values remain low, although they do not decrease further from ~7 Ma onward.

Downhole γ-ray measurements (Fig. 2) are often used to detect unconformities associated with low sea level stands (Haq et al., 1987). However, the variable glauconitic sand content in the RVG cores complicates the confident detection of regional unconformities using γ-ray in these shelfal settings. Hence, the palynological assemblages are the primary basis on which we based our sea-level reconstructions. The dinocyst record is characterized by a long-term decrease of the restricted marine and coastal taxa (RC index, Fig. 6A). Specifically, the SST$_{dino}$ shows cooling phases of increasing amplitude and duration. The generally higher pollen abundance relative to dinocysts (P/D index) at the inshore GH site clearly demonstrates the more

proximal setting relative to the more offshore HEU borehole, while the RC index is comparable at both sites. Both cores reveal a series of sea level variations superimposed on the long-term shallowing trend, which, in GH, is followed by a strong increase in the P/D index to around 50% in the uppermost part related to the progradation of fluvial deposits from the paleo-Rhine delta (Geluk et al., 1994).

6. Discussion

6.1. Marine and terrestrial climatic trends

The cooling phases in the TT$_{pollen}$ reconstruction (Fig. 5d) mirror the pronounced cooling trends seen in the winter temperature reconstruction of Mosbrugger et al. (2005) (cold month mean, CMM in Fig. 5a), which they attribute to increased seasonal contrast. Subtropical vegetation elements are particularly sensitive to lowering of annual minimum temperatures. For example, late Pliocene pollen records from Italy (Semaforo, Calabria) and Germany (Lieth) have shown that obliquity-forced winter cooling causes pollen assemblages

Table 2
Dinocyst biostratigraphy of GH and HEU boreholes.

Dinocyst HO (LO)	Borehole depth (m)		Age (Ma)	Chron
	GH	HEU	GTS 2004	(top)
Reticulatosphaera actinocoronata abundant, *Melitasphaeridium choanophorum, Barssidinium pliocenicum,* and *Operculosphaeridium tegillatum* present	83		~5	n.a.
Labyrinthodinium truncatum	103	111	7.53	C4n.1n
Systematophora placacantha	109	123	8.11	C4r.1r
Palaeocystodinium golzowense	127	134	8.77	C4An
Cannosphaeropsis passio	148	161	11.04	C5r.1r
Cerebrocysta poulsenii	196	216	11.80	Mid C5r.3r
Achomosphaera andalousiensis (LO)	196	216	12.21	C5An.2n
Unipontidinium aquaeductum	202	246	12.42	C5Ar.1r
Palaeocystodinium ventricosum	207	258	13.02	C5AAn
Cousteaudinium aubryae, Distatodinium paradoxum	258	285	14.88	C5Bn.1r
Unipontidinium aquaeductum (LO)	274	308	15.16	C5Br
Labyrinthodinium truncatum (LO), *Cerebrocysta poulsenii* (LO)	292	327	15.80	Lower C5Br
Cordosphaeridium cantharellum	321	355	17.53	C5Dr.1r

Correlations between chrons and dinocyst events are taken from Munsterman and Brinkhuis (2004) and updated to the GTS 2004 (Lourens et al., 2004).

to change (Pross and Klotz, 2002; Klotz et al., 2006). Subtropical humid elements were shown to be sensitive to changes in temperature rather than in precipitation, since reconstructed winter temperatures decreased while humidity levels remained relatively constant. Hence, the trends towards lower temperatures in our TT_{pollen} record is the likely result from winter cooling and increased seasonal contrast.

The MBT/CBT proxy provides mean terrestrial temperature estimates for the Middle Miocene Climatic Optimum, between 13.5 and 17 Ma, of ~24.5 °C, with maxima reaching up to 28 °C. MAT estimates based on the fossil floras are lower and range up to 21 °C for the middle Miocene (Mosbrugger et al., 2005). Other estimates, e.g. based on fossil wood assemblages and $\delta^{18}O$ values of freshwater organisms (Table 3), range between 20 and 22 °C (Tütken et al, 2006; Böhme et al., 2007). Although the absolute temperature estimates based on the rather new MBT/CBT proxy are still associated with a relatively large calibration error of 5 °C, the maximum middle Miocene TT_{GDGT} estimates of up to 27 °C seem to exceed other available quantitative proxy data (Table 3). A potential explanation could be a seasonal bias in any of the proxies. Although no seasonal bias has been detected in the MBT/CBT soil calibration set (Weijers et al., 2007b), a potential bias in the TT_{GDGT} estimates in this record toward wetter or warmer seasons, when microbial activity is likely higher, can at this stage not be excluded. Vegetation-based temperature estimates, however, are more sensitive

to winter season temperature, which is the most limiting factor for subtropical vegetation (e.g., Pross and Klotz., 2002; Klotz et al., 2006). The late Miocene (Messinian) TT_{GDGT} estimate of 14–16 °C is more consistent with other available records, such as 13.5–16.3 °C based on the fossil floras reported by Mosbrugger et al. (2005) (Table 3). Thus, during the gradual Miocene cooling trend, the different temperature estimates converge. Potentially, a more equal distribution of precipitation over the seasons might cause the TT_{GDGT} estimates to be more representative of the annual signal, whereas introduction of more temperate vegetation taxa might result in a temperature estimation that is less sensitive toward winter season temperatures. Experimental evidence shows that plants are more sensitive to cold conditions under elevated levels of atmospheric $[CO_2]$ (Royer et al., 2000). A recent reconstruction of high, early to middle Miocene atmospheric $[CO_2]$ (Kürschner et al., 2008) therefore implies that the climatic ranges of extant plants that grow under current ambient $[CO_2]$, used by Mosbrugger et al. (2005) to estimate paleotemperatures, are possibly biased towards colder conditions relative to the fossil floras growing under elevated $[CO_2]$.

Both the TT_{pollen} and the CMM reconstruction of Mosbrugger et al. (2005) show relatively stable temperatures during the Langhian, followed by a Serravallian cooling (Fig. 5a, d). However, the start of cooling phase III seems offset between both curves since the Mosbrugger et al. (2005) reconstruction is based on interpolation of data between 8 and 11 Ma. The TT_{GDGT} temperature reconstruction corresponds largely to the cooling trend seen in TT_{pollen}, although it shows an overall higher variability (Fig. 5c, e). An exception is the short warming around ~7.2 Ma seen in the TT_{GDGT}. The 8.6–6.6 Ma interval of the TT_{GDGT} data shows greater correspondence to the pollen-derived humidity index (TH_{pollen}). The latter is largely controlled by the abundance of *Taxodiaceae*, which is typical of swamp vegetation, but also reflects warm conditions. Hence, the temperature increase around 7.4 Ma seen in the CMM and TT_{GDGT} data is likely a realistic feature.

In the Mosbrugger et al. (2005) mean annual precipitation record (MAP, Fig. 5b), humidity levels are relatively stable until the Zanclean (~5 Ma), whereas the TH_{pollen} record of GH indicates a change towards drier conditions at ca. 7.5 Ma. This large temporal offset is unlikely to be an effect of dating uncertainties. Most likely, the offset reflects differences in regional swamp development in response to tectonic or sea-level changes.

In contrast to the gradual cooling evident from the terrestrial temperature proxies, the SST_{dino} record is expressed as periodical influxes of cold-water taxa. The different signatures of the terrestrial and marine temperature records (Fig. 5) might be due to different responses and seasonality of the proxies. At mid latitudes, dinoflagellates typically bloom in spring, early summer or early autumn (Dale, 1996). Hence, our SST_{dino} records are considered to represent mainly warm-season temperatures, in contrast to the winter-

Table 3
Average reconstructed terrestrial MAT estimates for Europe during the Miocene.

Period	Age (Ma)	Region	MAT (°C)	Method	Reference
Early Pliocene	5.4–3	SW Germany	14	MBT/CBT	*this study*
		Central Europe	13	Seeds, fruits and leaves	Mosbrugger et al. (2005)
Late Miocene	11.2–5.4	SW Germany	20	MBT/CBT	*this study*
		Central Europe	16	Seeds, fruits and leaves	Mosbrugger et al. (2005)
		Central Europe	15	Thermophilic ectothermic vertebrates	Böhme (2003)
Middle Miocene	16–13	SW Germany	25	MBT/CBT	this study
Climatic Optimum		South Germany	18	Fossil wood flora	Böhme et al. (2007)
		SW Germany	~20	$\delta^{18}O$ fossil teeth and freshwater microorganisms	Tütken et al. (2006)
		Central Europe	18	Seeds, fruits and leaves	Mosbrugger et al. (2005)
		Central Europe	>22	Bauxite, fossil wood, ectothermic vertebrates	Böhme (2003)
'First Climatic Optimum'	16.5–16.3	SW Germany	27	MBT/CBT	*this study*
		South Germany	23	Fossil wood flora	Böhme et al. (2007)
Early Miocene	23.8–18	Central Europe	18	Seeds, fruits and leaves	Mosbrugger et al. (2005)

temperature controlled terrestrial pollen record. The apparent smoothed nature of the pollen record is in part due to transport processes whereby signals from a relatively large catchment (Lower Rhine Graben) are integrated and thereby averaged. More importantly however, the maximum cooling pulses evident from the SST$_{dino}$ and — to a lesser degree — the bacterially-derived TT$_{GDGT}$ records (Fig. 5g, h) most likely represent relatively short-term climate 'events' such as high latitude glaciations that cause irreversible changes in the vegetation, which is reflected in the pollen assemblages as a cooling with no return to warm conditions.

Based on comparison of terrestrial temperature data and the global compilation curve of benthic δ^{18}O records (Zachos et al., 2001), Mosbrugger et al. (2005) conclude that a 2-million year offset and, thus, a decoupling between land and sea climate occurs around the mid-Miocene cooling event. Our integrated TT$_{pollen}$, TT$_{GDGT}$, and SST$_{dino}$ records do not support such a conclusion. Despite the aforementioned different characteristics of the proxy records, the long-term climatic trends in our data are largely comparable and point to a single climatic forcing mechanism, influencing land and sea concomitantly.

6.2. Climate and sea level

The first cooling signal at ~14 Ma in our terrestrial and marine palynological data (I and IV in Fig. 5) most likely represents the middle Miocene global cooling, which is widely recorded as a benthic foraminiferal δ^{18}O increase between 14.8 and 13.6 Ma, and is commonly associated with the expansion of the East Antarctic ice-sheet (see Flower and Kenneth, 1994; Miller et al., 1991; Zachos et al., 2001; Holbourn et al., 2005). The main middle Miocene expansion of the Antarctic ice-sheet occurred at ~13.8–13.9 Ma, which has been attributed to low insolation under declining atmospheric [CO$_2$] levels (Abels et al., 2005). A minimum obliquity orbital configuration probably promoted ice-sheet growth by causing a high latitudinal gradient in summer insolation, which drives the poleward atmospheric heat and moisture transfer needed for the build-up of ice (Holbourn et al., 2005).

We compared the short-scale changes in the GH and HEU proxy records with the timing of Miocene (Mi) glacial stages identified by Miller et al. (1991, 1996; see also 2005) in a benthic foraminiferal δ^{18}O record from Deep Sea Drilling Project (DSDP) site 608 in the North-East Atlantic (Fig. 5i). Orbitally-tuned age estimates for several of the Mi glacials from other records are given in Fig. 5j. As expected, the more distal and expanded HEU SST$_{dino}$ record shows the most pronounced cooling signal, particularly around 9.5 Ma. The majority of the SST$_{dino}$ coolings (Fig. 5g, h) is consistent with the orbitally-tuned Mi glaciations (Fig. 5j). Only the Mi-6 glacial is not represented and a small additional cooling is seen around 12 Ma in both the SST$_{dino}$ and TT$_{GDGT}$. The most prominent SST$_{dino}$ decrease, during the late Tortonian (Fig. 5g, h), is concurrent with the disappearance or regional extinction of subtropical floral elements of pollen zone GH IV (see supplementary Fig. 3), which is reflected as a significant decrease in TT$_{pollen}$ (Fig. 5d). The prominent cooling pulse in our record does apparently not correlate to a formal Mi-glacial event, although benthic foraminiferal δ^{18}O values after Mi-7 remain high until ~7.5 Ma (e.g. Miller et al., 1991; Zachos et al., 2001, Fig. 5i), coincident with the end of the prominent SST$_{dino}$ cooling pulse. Either the late Tortonian benthic foraminiferal δ^{18}O signature has not been constrained well or, alternatively, the SST$_{dino}$ signal is largely regional and not related to a global glaciation, which would also explain why sedimentation at the inshore GH site was not interrupted by a sea-level lowering during cooling.

An SST decrease between ~9.5 and 8 Ma has also been observed in planktonic foraminifera assemblage data from astronomically tuned sections in the eastern and central Mediterranean (Gavdos Island and Southern Sicily, respectively) (Lourens and Hilgen, 1997; Turco et al., 2001). In agreement with our SST$_{dino}$ record, the distinct cold phase at Gavdos Island is followed by warming, indicative of a widespread climatic event. The SST changes in the Mediterranean

have been related to an obliquity amplitude minimum and maximum eccentricity orbital configuration (Lourens and Hilgen, 1997; Turco et al., 2001), which implies a relation with glacial stages, although no distinct benthic foraminiferal δ^{18}O event has yet been recognized (Fig. 5).

Since the SST$_{dino}$ signals are largely consistent with Mi glaciations they most likely coincide with global eustatic sea level variations. Levels A-I in Fig. 6 highlight coolings in the SST$_{dino}$ at HEU and/or increased pollen input at GH that are consistent with lower sea levels. The long-term trend in the BIT index confirms the changes in the relative amount of terrestrial palynomorphs (Figs. 5, 6). Notably, most levels A-I also correspond to reduced relative amounts of dinocysts indicative of restricted and shallow conditions (RC index) at both HEU and GH. This counter-intuitive change can be explained by the geographical setting of the GH and HEU boreholes. Both sites are adjacent to relatively elevated tectonic blocks (Peel and Krefeld Blocks, see Fig. 1). During sea level lowstands, these areas are most likely at or above sea level, as evidenced by extensive hiati in the sedimentary record on the elevated Peel Block (Wijnker et al., 2008). Rising sea level floods these areas and actually expands the area typical for restricted and shallow marine dinocysts for both sites. The clearly higher *P/D* index and more proximal setting at GH shows that, relative to HEU, GH receives more terrestrial run-off. Due to this particular environmental setting, the decreases in the pollen input (lower *P/D*) seen in Fig. 6 are consistent with greater abundance of restricted dinocysts (higher RC) due to increasing shelf area.

Interpretation of the sea-level signal is complex, and hampered by the lack of detailed age dating. Within the age uncertainties of our records and the most recent global sea-level compilation of Miller et al. (2005) (Fig. 6) the approximate number and spacing of the North Sea sea-level minima (A-I in Fig. 6) can be made to agree. The majority of the global sea-level curve is based on backstripping of New Jersey shelf sediments, and has an age uncertainty of ~0.5 Ma (Miller et al., 2005). Hence, any detailed correlations should be treated with caution since most sea level variations shown in Fig. 6 are in the order of 10^5 years in duration. This aspect of our study needs further high resolution data and better age control. It is notable, however, that little sea-level lowering is seen during the most prominent SST$_{dino}$ signal (B in Fig. 6), again pointing to a mostly regional cooling.

7. Conclusions

A detailed land-sea correlation on the basis of a Miocene palynological record from the North Sea Basin reveals a coupled climate system between the NW European marine and terrestrial realms. Both palynological and organic geochemical methods reveal the general long term cooling trend for the mid to late Miocene. Using the MBT/CBT proxy, the maximum cooling for this time period is estimated to be ca. 13 °C. An additional 4 °C cooling is estimated for the early Pliocene. A two-million year time lag between terrestrial and marine temperature changes in the middle Miocene, as proposed by Mosbrugger et al. (2005), is not supported by these new data. The terrestrial climate changes reconstructed here are more gradual compared to the pulsed sea-surface coolings (SST$_{dino}$) in the North Sea Basin, although the pollen signal is possibly less responsive to short-term warmings. Glacial Mi-events known from benthic foraminiferal δ^{18}O records are generally reflected by the SST$_{dino}$ decreases, which increase in amplitude during the Miocene. An additional strong cool phase from ~8.4 Ma in both the terrestrial and marine signal from the North Sea Basin seems unrelated to defined deep-sea benthic δ^{18}O stages. Since the timing of Mi-7 is not resolved (Westerhold et al., 2005), and the general detection of Mi-stages is complicated, a benthic δ^{18}O glacial around 8.4 Ma has possibly not yet been detected.

The shallow marine palynological and organic-geochemical records are shown to be valuable for both paleoclimatic and stratigraphical purposes, especially for understanding the exact coupling between

marine and terrestrial systems and replace outdated regional terrestrial-based zonation (Donders et al., 2007).

Acknowledgments

Appendix A. Supplementary data

Supplementary data associated with this article can be found, in the online version, at doi:10.1016/j.epsl.2009.02.034.

References

Abels, H.A., Hilgen, F.J., Krijgsman, W., Kruk, R.W., Raffi, I., Turco, E., Zachariasse, W.J., 2005. Long-period orbital control on middle Miocene global cooling: integrated stratigraphy and astronomical tuning of the Blue Clay Formation on Malta. Paleoceanography 20, PA4012.

Andersson, C., Jansen, E., 2003. A Miocene (8–12) intermediate water benthic stable isotope record from the northeastern Atlantic, ODP Site 982. Paleoceanography 18 (1), 1013.

Berggren, W.A., Kent, D.V., Swisher III, C.C., Aubry, M.-P., 1995. A revised Cenozoic geochronology and chronostratigraphy. In: Berggren, W.A., Kent, D.V., Hardenbol, J. (Eds.), Geochronology, Time Scales and Global Stratigraphic Correlation. SEPM (Society for Sedimentary Geology). Special Publication, vol. 54. Tulsa, Oklahoma, USA, pp. 129–212.

Birks, H.J.B., Birks, H.H., 1980. Quaternary Palaeoecology. Edward Arnold, London. 289 pp.

Böhme, M., 2003. The Miocene Climatic Optimum: evidence from ectothermic vertebrates of Central Europe. Palaeogeogr., Palaeoclimatol., Palaeoecol. 195, 389–401.

Böhme, M., Bruch, A.A., Selmeier, A., 2007. The reconstruction of Early and Middle Miocene climate and vegetation in Southern Germany as determined from the fossil wood flora. Palaeogeogr., Palaeoclimatol., Palaeoecol. 253, 91–114.

Brinkhuis, H., 1994. Late Eocene to early Oligocene dinoflagellate cysts from the Priabonian type-area (Northeast Italy); biostratigraphy and palaeoenvironmental interpretation. Palaeogeogr., Palaeoclimatol., Palaeoecol. 107, 121–163.

Brinkhuis, H., Schiøler, P., 1996. Palynology of the Geulhemmerberg Cretaceous/Tertiary boundary section (Limburg, SE Netherlands). In: H.S. Brinkhuis, J. (Ed.), The Geulhemmerberg Cretaceous/Tertiary boundary section (Maastrichtian type area, SE Netherlands). Geologie en Mijnbouw, pp. 193–213.

Dale, B., 1996. Dinoflagellate cyst ecology: modelling and geological applications. In: Jansonius, J., McGregor, D.C. (Eds.), Palynology: principles and applications. American Association of Stratigraphic Palynologists Foundation, Dallas, Texas, pp. 1249–1275.

Donders, T.H., Kloosterboer-van Hoeve, M.L., Westerhoff, W., Verreussel, R.M.C.H., Lotter, A.F., 2007. Late Neogene continental stages in NW Europe revisited. Earth Sci Rev 85 (3–4), 161–186.

Doppert, J.W.C., Ruegg, G.H.J., Van Staalduinen, C.J., Zagwijn, W.H., Zandstra, J.G., 1975. Formaties van het Kwartair en het Boven-Tertiair in Nederland. In: Zagwijn, W.H., Van Staalduinen, C.J. (Eds.), Toelichting bij geologische overzichtskaarten van Nederland. Rijks Geologische Dienst, Haarlem, pp. 11–56.

Dybkjaer, K., 2004. Dinocyst stratigraphy and palynofacies studies used for refining a sequence stratigraphic model-uppermost Oligocene to lower Miocene, Jylland, Denmark. Rev. Palaeobot Palynol. 131, 201–249.

Fauquette, S., Guiot, J., Suc, J.-P., 1998. A method for climatic reconstruction of the Mediterranean Pliocene using pollen data. Palaeogeogr., Palaeoclimatol., Palaeoecol. 144, 183–201.

Fensome, R.A., Williams, G.L., 2004. The Lentin and Williams index of fossil dinoflagellates, 2004 Edition. AASP Contributions Series, vol. 42. American Association of Stratigraphic Palynologists Foundation. 909 pp.

Flower, B.P., Kennett, J.P., 1994. The middle Miocene climatic transition: East Antarctic ice sheet development, deep ocean circulation and global carbon cycling. Palaeogeogr., Palaeoclimatol., Palaeoecol. 108, 537–555.

Geluk, M.C., Duin, E.J.T., Dusar, M., Rijkers, R.H.B., Van den Berg, M.W., Van Rooijen, P., 1994. Stratigraphy and tectonics of the Roer Valley Graben. Neth. J. Geosci./Geologie en Mijnbouw 73, 129–141.

Haq, B.U., Hardenbol, J., Vail, P.R., 1987. Chronology of fluctuating sea levels since the Triassic (250 million years ago to the present). Science 235, 1156–1167.

Head, M.J., 1998. Marine environmental change in the Pliocene and early Pleistocene of eastern England: the dinoflagellate evidence reviewed. Meded. Nederlands Instituut voor Toegepaste Geowetenschappen TNO 60, 199–226.

Holbourn, A., Kuhnt, W., Schulz, M., Erlenkeuser, H., 2005. Impacts of orbital forcing and atmospheric carbon dioxide on Miocene ice-sheet expansion. Nature 438 (7067), 483.

Hooghiemstra, H., 1988. Palynological records from Northwest African marine sediments: a general outline of the interpretation of the pollen signal. Philos. Trans. R. Soc. Lond., Series B Biol. Sci. 318 (1191), 431–449.

Hopmans, E.C., Schouten, S., Pancost, R.D., Van der Meer, M.T.J., Sinninghe Damsté, J.S., 2000. Analysis of intact tetraether lipids in archaeal cell material and sediments by high performance liquid chromatography/atmospheric pressure chemical ionization mass spectrometry. Rapid Commun. Mass Spectrom. 14, 585–589.

Hopmans, E.C., Weijers, J.W.H., Schefuß, E., Herfort, L., Sinninghe Damsté, J.S., Schouten, S., 2004. A novel proxy for terrestrial organic matter in sediments based on branched and isoprenoid tetraether lipids. Earth Planet. Sci. Lett. 224, 107–116.

Huhn, B., Utescher, T., Ashraf, A.R., Mosbrugger, V., 1997. The peat-forming vegetation in the Middle Miocene Lower Rhine Embayment, an analysis based on palynological data. Meded. Nederlands Instituut voor Toegepaste Geowetenschappen TNO 58, 211–218.

Kemna, H.A., Westerhoff, W.E., 2007. Remarks on the palynology-based chronostratigraphic subdivision of the Pliocene terrestrial deposits in NW-Europe. Quat. Int. 164–165, 184–196.

Klotz, S., Fauquette, S., Combourieu-Nebout, N., Uhl, D., Suc, J.-P., Mosbrugger, V., 2006. Seasonality intensification and long-term winter cooling as a part of the late Pliocene climate development. Earth Planet. Sci. Lett. 241 (1–2), 174–187.

Köthe, A., Piesker, B., 2007. Stratigraphic distribution of Paleogene and Miocene dinocysts in Germany. Revue de Paléobiologie 26 (1), 1–39.

Kürschner, W.M., Kvaček, Z., Dilcher, D.L., 2008. Proc. Nat. Acad. Sci. U S A. 105 (2), 449–453.

Lourens, L., Hilgen, F., Shackleton, N.J., Laskar, J., Wilson, D., 2004. The Neogene Period. In: Gradstein, F.M., Ogg, J.G., Smith, A.C. (Eds.), A Geologic Time Scale 2004. Cambridge University Press, Cambridge, pp. 409–440.

Lourens, L.J., Hilgen, F.J., 1997. Long-periodic variations in the earth's obliquity and their relation to third-order eustatic cycles and late Neogene glaciations. Quat Int. 40, 43–52.

Lücke, A., Helle, G., Schleser, G.H., Figueiral, I., Mosbrugger, V., Jones, T.P., Rowe, N.P., 1999. Environmental history of the German Lower Rhine Embayment during the middle Miocene as reflected by carbon isotopes in brown coal. Palaeogeogr., Palaeoclimatol., Palaeoecol. 154, 339–352.

Menke, B., 1976. Pliozane und altestquartare Sporen- und Pollenflora von Schleswig-Holstein. Geologisches Jahrbuch, A 32, 3–197.

Miller, K.G., Fairbanks, R.D., Thomas, E., 1986. Benthic foraminiferal carbon isotopic records and the development of abyssal circulation in the eastern North Atlantic. Init. Reports Deep Sea Drilling Project 94, 981–996.

Miller, K.G., Kominz, M.A., Browning, J.V., Wright, J.D., Mountain, G.S., Katz, M.E., Sugarman, P.J., Cramer, B.S., Christie-Blick, N., Pekar, S.F., 2005. The phanerozoic record of global sea-level change. Science 310 (5752), 1293–1298.

Miller, K.G., Mountain, G.S., the Leg 150 Shipboard Party, n. and Members of the New Jersey Coastal Plain Drilling Project, n., 1996. Drilling and dating New Jersey Oligocene–Miocene sequences: ice volume, global sea level, and Exxon records. Science 271 (5252), 1092–1095.

Miller, K.G., Wright, J.D., Fairbanks, R.D., 1991. Unlocking the Ice House: Oligocene–Miocene oxygen isotopes, eustacy and margine erosion. J. Geophys. Res. 96 (B4), 6829–6848.

Mohr, B.A.R., 1986. Die Mikroflora der Oberpliozanen Tone von Willershausen (Kreis Northeim, Niedersachsen). Palaeontogr. Abt. B 198 (3–6), 133–156.

Mosbrugger, V., Utescher, T., Dilcher, D.L., 2005. Cenozoic continental climatic evolution of Central Europe. Proc. Natl. Acad. Sci. USA 102 (42), 14964–14969.

Munsterman, D.K., Brinkhuis, H., 2004. A southern North Sea Miocene dinoflagellate cyst zonation. Neth. J. Geosci./Geologie en Mijnbouw 83 (4), 267–285.

Pross, J., Brinkhuis, H., 2005. Organic-walled dinoflagellate cysts as paleoenvironmental indicators in the Paleogene; a synopsis of concepts. Paläontol. Z. 79 (1), 53–59.

Pross, J., Klotz, S., 2002. Palaeotemperature calculations from the Praetiglian/Tiglian (Plio-Pleistocene) pollen record of Lieth, northern Germany: implications for the climatic evolution of NW Europe. Global Planet. Change 34, 253–267.

Royer, D.L., Osborne, C.P., Beerling, D.J., 2000. High CO_2 increases the freezing sensitivity of plants: implications for paleoclimatic reconstructions from fossil floras. Geology 30 (11), 963–966.

Schouten, S., Hopmans, E.C., Pancost, R.D., Sinninghe Damsté, J.S., 2000. Widespread occurrence of structurally diverse tetraether membrane lipids: evidence for the ubiquitous presence of low-temperature relatives of hyperthermophiles. Proc. Nat. Acad. Sci. U. S. A. 97, 14421–14426.

Schouten, S., Hopmans, E.C., Schefuß, E., Sinninghe Damsté, J.S., 2002. Distributional variations in marine crenarchaeotal membrane lipids: a new tool for reconstructing ancient sea water temperatures? Earth Planet. Sci. Lett. 204 (1–2), 265–274.

Schouten, S., Huguet, C., Hopmans, E.C., Kienhuis, M.V.M., Sinninghe Damsté, J.S., 2007. Analytical methodology for TEX86 paleothermometry by high-performance liquid chromatography/atmospheric pressure chemical ionization–mass spectrometry. Anal. Chem. 97 (7), 2940–2944.

Shackleton, N.J., Crowhurst, S.J., Weedon, G.P., Laskar, J., 1999. Astronomical calibration of Oligocene–Miocene times. Phil. Trans. Royal Soc. Lond.: Math., Phys. Eng. Sci., A 357, 1907–1929.

Sinninghe Damsté, J.S., Ossebaar, J., Verschuren, D., Schouten, S., 2008. Altitudinal shifts in the branched tetraether lipid distribution in soil from Mt. Kilimanjaro (Tanzania): implications for the MBT/CBT continental palaeothermometer. Org. Geochem. 39, 1072–1076.

Sluijs, A., Pross, J., Brinkhuis, H., 2005. From greenhouse to icehouse; organic walled dinoflagellate cysts as paleoenvironmental indicators in the Paleogene. Earth-Sci Rev 68, 281–315.

Stover, L.E., Brinkhuis, H., Damassa, S.P., De Verteuil, L., Helby, R.J., Monteil, E., Partridge, A.D., Powell, A.J., Riding, J.B., Smelror, M., Williams, G.L., 1996. Mesozoic-tertiary dinoflagellates, acritarchs and prasinophytes. In: Jansonius, J., McGregor, D.C. (Eds.), Palynology, Principles and Applications. AASP Foundation, pp. 641–750.

Stuchlik, L. (Ed.), 2002. Atlas of Pollen and Spores of the Polish Neogene. Gymnosperms. W. Szafer Institute of Botany, vol. 2. Polish Academy of Sciences, Kraków. 237 pp.

Suc, J.-P., Zagwijn, W.H., 1983. Plio-Pleistocene correlations between the northwestern Mediterranean region and northwestern Europe according to recent biostratigraphic and palaeoclimatic data. Boreas 3, 153–166.

Traverse, A., 1988. Paleopalynology. Unwin Hyman, Boston. 600 pp.

Turco, E., Hilgen, F., Lourens, L., Shackleton, N.J., Zachariasse, J.W., 2001. Punctuated evolution of global climate cooling during the late Middle to early late Miocene: high-resolution planktonic foraminiferal and oxygen isotope records from the Mediterranean. Paleoceanography 16 (4), 405–423.

Tütken, T., Vennemann, W., Janz, H., Heizmann, E.P.J., 2006. Palaeoenvironment and palaeoclimate of the middle Miocene lake in the Steinheim basin, SW Germany: a reconstruction from C, O, and Sr isotopes of fossil remains. Palaeogeogr., Palaeoclimatol., Palaeoecol. 241, 457–491.

Utescher, T., Mosbrugger, V., Ashraf, A.R., 2000. Terrestrial climate evolution in Northwest Germany over the last 25 million years. Palaios 15, 430–449.

Van den Berg, M.W., 1994. Neotectonics of the Roer Valley rift system. Style and rate of crustal deformation inferred from syntectonic sedimentation. Neth. J. Geosci./Geologie en Mijnbouw 73, 143–156.

Versteegh, G.J.M., Zonneveld, K.A.F., 1994. Determination of (palaeo-)ecological preferences of dinoflagellates by applying detrended and canonical correspondence analysis to late Pliocene dinoflagellate cyst assemblages of the south Italian Singha section. Rev. Palaeobot. Palynol. 84, 181–199.

Weijers, J.W.H., Schouten, S., Hopmans, E.C., Geenevasen, J.A.J., David, O.R.P., Coleman, J.M., Pancost, R.D., Sinninghe Damsté, J.S., 2006a. Membrane lipids of mesophilic anaerobic bacteria thriving in peats have typical archaeal traits. Environ. Microbiol. 8, 648–657.

Weijers, J.W.H., Schouten, S., Spaargaren, O.C., Sinninghe Damsté, J.S., 2006b. Occurrence and distribution of tetraether membrane lipids in soils: implications for the use of the TEX$_{86}$ proxy and the BIT index. Org. Geochem. 37, 1680–1693.

Weijers, J.W.H., Schefuß, E., Schouten, S., Sinninghe Damsté, J.S., 2007a. Coupled thermal and hydrological evolution of tropical Africa over the last deglaciation. Science 315, 1701–1704.

Weijers, J.W.H., Schouten, S., Van den Donker, J.C., Hopmans, E.C., Sinninghe Damsté, J.S., 2007b. Environmental controls on bacterial tetraether membrane lipid distribution in soils. Geochim. Cosmochim. Acta 71, 703–713.

Westerhold, T., Bickert, T., Röhl, U., 2005. Middle to late Miocene oxygen isotope stratigraphy of ODP site 1085 (SE Atlantic): new constrains on Miocene climate variability and sea-level fluctuations. Palaeogeogr., Palaeoclimatol., Palaeoecol. 217 (3–4), 205–222.

Whitehead, D.R., 1983. Wind pollination: some ecological and evolutionary perspectives. In: Real, L. (Ed.), Pollination Biology. Academic Press, Orlando, pp. 97–108.

Wijnker, E., Bor, T.J., Wesselingh, F.P., Munsterman, D.K., Brinkhuis, H., Burger, A.W., Vonhof, H.B., Post, K., Hoedemakers, K., Janse, A.C., Taverne, N., 2008. Neogene stratigraphy of the Langenboom locality (Noord-Brabant, the Netherlands). Neth. J. Geosci. 87 (2), 165–180.

Wood, G.D., Gabriel, A.M., Lawson, J.C., 1996. Palynological techniques — processing and microscopy. In: Jansonius, J., McGregor, D.C. (Eds.), Palynology: principles and applications. AASP, Salt Lake City, pp. 29–50.

Zachos, J., Pagani, M., Sloan, L., Thomas, E., Billups, K., 2001. Trends, rhythms, and aberrations in global climate 65 Ma to present. Science 292, 686–693.

Zachos, J.C., Dickens, G.R., Zeebe, R.E., 2008. An early Cenozoic perspective on greenhouse warming and carbon-cycle dynamics. Nature 451 (7176), 279–283.

Zagwijn, W.H., Hager, H., 1987. Correlations of continental and marine Neogene deposits in the south-eastern Netherlands and the Lower Rhine District. Meded. Werkgr. Tert. Kwart. Geol. 24 (1–2), 59–78.

Zevenboom, 1988. Dinoflagellate cysts from the Mediterranean Late Oligocene and Miocene. Ph.D. Dissertation Utrecht University, p. 221.

Ziegler, P.A., 1994. Cenozoic rift system of western and central Europe: an overview. Neth. J. Geosci./Geologie en Mijnbouw 73, 99–127.